Applied Microbiology and Biotechnology (2024) 108:474
https://doi.org/10.1007/s00253-024-13311-2

BIOTECHNOLOGICALLY RELEVANT ENZYMES AND PROTEINS

Enhancing the imidase activity of BpIH toward 3-isobutyl glutarimide via semi-rational design

Wenping Qin[1,2] · Long Xu[3] · Kun Cheng[1] · Yinhua Lu[2] · Zhongyi Yang[1]

Received: 23 June 2024 / Revised: 3 September 2024 / Accepted: 16 September 2024 / Published online: 25 September 2024

Abstract

(*R*)-3-Isobutylglutarate monoamide (*R*-IBM) is a key intermediate in the synthesis of the analgesic drug pregabalin. Recently, the imidase BpIH derived from *Burkholderia phytofirmans* was identified as a promising catalyst for the industrial production of *R*-IBM. Notably, this catalyst has the distinct advantage of achieving a 100% theoretical yield from 3-isobutyl glutarimide (IBI). In this study, homology modeling and structure alignment techniques were used to determine the substrate binding pocket of BpIH. Semi-rational design was used to analyze the amino acid residue conservation in the binding pocket region of BpIH. Interestingly, mutations of several low-conserved amino acid located 6–9 Å from the substrate significantly enhanced the catalytic activity of BpIH. Among them, the triple mutant Y37FH133NS226I (YHS-I) showed approximately a fivefold increase in enzyme activity and a significantly improved catalytic efficiency (k_{cat}/*K*m). Under the same reaction time and conditions, YHS-I successfully converted IBI into *R*-IBM with a conversion rate of 88.87%, with an enantiomeric excess (*ee*) of the product exceeding 99.9%. In comparison, wild-type BpIH had a conversion rate of only 38.15%. Molecular dynamics and docking results indicated that YHS-I had higher rigidity around the mutation sites. The synergistic substitutions of Y37F, H133N, and S226I altered the interaction network within the mutation site, enhancing the protein's affinity for the substrate and improving catalytic efficiency.

Key points

- *100% theoretical yield of R-IBM by BpIH compared with 50% by resolution*
- *Semi-rational design of BpIH based on conservativity with homologous enzymes*
- *Mutant with enzyme activity of sixfold and product ee value of 99.9%*

Keywords Imidase · *R*-3-Isobutylglutarate monoamide (*R*-IBM) · Pregabalin · Semi rational design · Directed evolution

Introduction

(*S*)-3-Aminomethyl-5-methylhexanoic acid, also known as pregabalin, is a structural analog of gamma-aminobutyric acid (GABA). Pregabalin is used for the treatment of various central nervous system disorders, including neuropathic pain, epilepsy, and anxiety-related autism (Gray 2007; Silverman 2008; Tassone et al. 2007). When administered orally, pregabalin is rapidly absorbed and transported specifically to the brain (Bockbrader et al. 2010). Compared to 3-alkyl-GABA analogs, pregabalin demonstrates greater effectiveness with fewer associated side effects. Consequently, there has been a notable increase in demand for pregabalin in recent years.

The synthesis of pregabalin typically involves the use of chiral intermediates derived from (*R*)-3-cyano-5-methylhexanoic acid, (*R*)-isobutylglutaric acid monoamide, and

✉ Yinhua Lu
yhlu@shnu.edu.cn

✉ Zhongyi Yang
yangzhyi@126.com

[1] School of Pharmaceutical Sciences, Taizhou University, 1139 Shifu Rd, Taizhou 318000, China

[2] College of Life Sciences, Shanghai Normal University, 100 Guilin Rd, Shanghai 200233, China

[3] Taizhou Dachen Pharmaceutical Co., Ltd, 17 Fifth Avenue, Linhai Zone, Zhejiang National Chemical & Pharmaceutical Base, Taizhou 317016, China

(*R*)-isobutylglutaric acid monoester. These intermediates are primarily obtained through chiral or enzymatic resolution of the corresponding racemic precursors, resulting in a maximum yield of 50%. Any remaining precursors are either discarded or recycled following resolution. In recent years, there has been a growing interest in the production of chiral pregabalin intermediates through desymmetrization, which can potentially achieve a theoretical yield of 100% for chiral intermediates. Increasingly more studies have focused on the synthesis of chiral (*R*)-3-isobutylglutarate monoamide (*R*-IBM) through the hydrolysis of the symmetrical substrate 3-isobutylglutarimide (IBI) using imidase or hydantoinase. This area of study has become a new research hotspot in the field (Cai et al. 2023; Liu et al. 2022; Nojiri et al. 2015, 2013) (Scheme 1).

Imidase (EC 3.5.2.16) is a member of the α/β-fold hydrolase superfamily (Holmquist 2000; Huang 2020), and it was named according to its high activity toward cyclic imides (Ogawa et al. 2019). In the taxonomy of enzymes, it belongs to the hydrolases acting on carbon–nitrogen bonds in cyclic amides (EC 3.5.2.-), which include dihydropyrimidinase, dihydroorotase, and allantoinase. Most of these enzymes are zinc-dependent or have a metal center. For example, the active site of dihydropyrimidinase consists of an aspartate, four histidine residues, a carboxylated lysine, and a zinc-bound water molecule, which are essential for the assembly of the binuclear metal center (Huang 2020; Martínez-Rodríguez et al. 2010; Meelua et al. 2023). Allantoinase PuuE is structurally a polysaccharide deacetylase, but the conserved Asp-His-His metal binding triad in the polysaccharide deacetylase family is replaced by Glu-His-Trp, resulting in the metal independence of PuuE (Ramazzina et al. 2008). In PuuE, His259 was proposed to perform a nucleophilic attack on the carbonyl carbon in the substrate, with Glu36 acting as a catalytic acid to stabilize the oxyanion intermediate and donate a proton to the N atom of the substrate, creating a leaving group (Ramazzina et al. 2008).

In 2015, Masutoshi Nojiri et al. successfully purified imidase BpIH (EC 3.5.2.16) from *Burkholderia phytofirmans* DSM17436 and expressed it in *Escherichia coli*, resulting in the production of *R*-IBM with a 95.3% enantiomeric excess. The enzyme was also found to be metal-independent (Nojiri et al. 2015). Yet to date, no pdb data have been reported on this enzyme. Our research group also expressed BpIH in *E. coli*, which produced *R*-IBM with a high enantiomeric excess of 99.9% (Cai et al. 2023). However, the enzyme exhibited low activity, leading to significant costs associated with enzyme preparation and prolonged reaction times. Consequently, there is a pressing need to elucidate the mechanism of BpIH enzyme to enhance its catalytic efficiency.

In recent years, computer-aided directed evolution techniques have been used to design proteins with specific properties (Wu et al. 2022), including enhanced enzyme activity (Min et al. 2021; Wu et al. 2018), improved stability (Chen et al. 2022; Xu et al. 2020), and enhanced stereoselectivity (Zheng et al. 2023). These advancements have significantly increased the efficiency of enzymatic processes in various industrial applications. In this study, we deduced the substrate binding pocket of BpIH through homology modeling and structural alignment and then mutated residues within 5 Å and 6–9 Å from the substrate molecule. The triple mutation Y37FH133NS226I (YHS-I), 6–9 Å from the substrate molecule, showed approximately a fivefold increase in enzyme activity, with the enantiomeric excess (*ee*) of the product exceeding 99.9%.

Materials and methods

Homology modeling and selection of mutations

The sequences of BpIH (GenBank: ACD16728.1) and allantoinase family proteins were obtained from the National Center for Biotechnology Information (NCBI: https://www.ncbi.nlm.nih.gov/). Homology modeling of BpIH was performed using the SWISS-MODEL website (Arnold et al. 2006), with the crystal structure of the polysaccharide deacetylase family protein (PDB ID: 3S6O) used as a template. The sequence identity between BpIH and the template was found to be 91.3%. To assess the quality of the protein structure models, SAVES v6.0 (https://saves.mbi.ucla.edu/) was used. A library of allantoinase PuuE sequences was

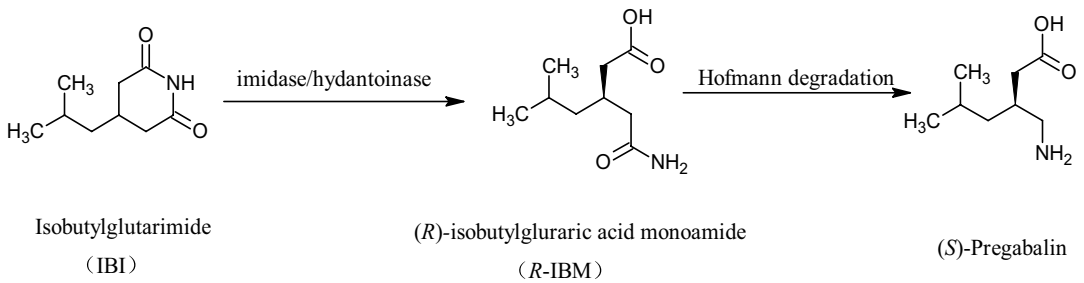

Scheme 1 Enzymatic desymmetrization of IBI and preparation of *S*-pregabalin

constructed. Multiple sequence comparisons of the library sequences were performed using CLUSTAL (Larkin et al. 2007), while multiple structure comparisons were carried out using PyMOL (http://www.pymol.org). Sequence conservation analysis was performed using the WebLogo server sequence library (Crooks et al. 2004).

To determine the binding site, substrate IBI was docked with BpIH using Autodock 4.0 following a similar procedure as previously reported (Jitonnom et al. 2012; Tue-Ngeun et al. 2024). Protein and IBI molecules were hydrogenated and charged, and a rigid protein structure was used. A genetic algorithm (GA) search method was used, the number of GA runs was 100, and the maximum number of evals was 5,000,000. The docking parameter was set to the default value. The center of the grid was (2.507, − 17.624, − 35.105), which was located in the middle of the E38-W131-H127 triad. The numbers of grid points in the x, y, and z directions were 111, 75, and 121, respectively. Then, 100 poses were generated and classified based on their binding sites, and the most likely binding site was selected based on the interaction of the substrate and surrounding residues. Then, the conformation with the highest score in this binding site was selected for further analysis (Morris et al. 2009). Residues surrounding IBI were selected for site-directed mutagenesis studies if they were ≤ 5 Å or 6–9 Å from the substrate.

Site-directed and site-saturation mutagenesis

The wild-type (WT) *BpIH* gene was synthesized with a C-terminal 6 × His tag and inserted into the *Nde*I and *Hin*dIII cleavage sites of plasmid pET30a(+). The resulting plasmid, named pT67, served as a DNA template for subsequent site-directed and site-saturation mutagenesis. Site-directed mutagenesis was performed using overlap extension PCR. The PCR product was then digested with *Dpn*I to eliminate any residual template. The primer pairs used in this study are listed in Table S1. Primers 1–56 were designed to substitute residues within 5 Å of the IBI region with alanine. Primers 57–86 were used for mutations of residues within 6–9 Å of the IBI region. Primers 87–106 were used for site-saturation mutations of residue S226. The mutations were confirmed by nucleotide sequencing, and the recombinant plasmid was transformed into *E. coli* BL21(DE3) competent cells.

Expression and purification of WT BpIH and its mutants

E. *coli* BL21(DE3) expressing WT BpIH protein or its mutants was cultured in LB medium supplemented with 50 μg mL^{-1} kanamycin at 37 °C. When the OD_{600} reached 0.6–0.8, the culture was induced with 0.5 mmol L^{-1} isopropyl-β-D-thiogalactoside (IPTG) for 14 h at 25 °C. The cells were collected by centrifugation at 10,000 *g* for 10 min, and 1.0 g of wet cells was resuspended with 3.0 mL of 10 mmol L^{-1} Tris–HCl (pH 8.0). A crude enzyme solution was obtained after sonification (50 W, 3 s on at 6-s intervals for 15 min and centrifugation at 10,000 *g* for 10 min). Then, protein purification was carried out according to the kit specifications (HyPur T Ni–NTA 6FF His-Tag PrePacked gravity column kit, Sangon Biotech Co., Ltd, Shanghai, China). The enzyme was eluted with 2 mL of elution buffer (50 mmol L^{-1} NaH_2PO_4, 300 mmol L^{-1} NaCl, 500 mmol L^{-1} imidazole, pH 8.0), and the fraction containing pure BpIH was collected. The eluted enzyme solution was concentrated using commercial ultrafiltration tubes (Merck, Germany) to obtain a concentrated purified enzyme solution of WT BpIH and its mutants. The purity and apparent molecular weight of the purified enzyme were estimated using a 12% SDS-PAGE gel. The concentration of the purified proteins was determined using a Bradford assay (Bradford 1976).

Enzyme activity assay and stability test

The biological activity of WT BpIH and its mutants was assessed by measuring the rate of conversion of IBI to the product IBM. The reaction was conducted in a 5-mL system containing 50 mmol L^{-1} Tris–HCl (pH 8.0), 10 mmol L^{-1} IBI, and 800 μL of an enzyme solution at a temperature of 40 °C for a duration of 30 min. After completing the reaction, the enzyme was deactivated by dilution with the mobile phase for high-performance liquid chromatography (HPLC) analysis. Enzyme activity was quantified in terms of units, where one unit represents the amount of enzyme required to produce 1 μmol of IBM per minute.

The stability of WT BpIH and its mutants was evaluated at a temperature of 40 °C. The enzyme solution was diluted by a factor of four with 50 mmol L^{-1} Tris–HCl buffer (pH 8.0) and incubated in a water bath at 40 °C. Protein samples were collected at regular intervals, and the enzyme activity was measured to assess the stability of the proteins under these conditions.

Kinetic analysis and bioconversion comparison

To determine the kinetic parameters of WT BpIH and different mutants, a volume of purified enzyme solution (200 μL, 0.27 μg $μL^{-1}$) was mixed with 2 mL of an IBI reaction solution at different concentrations (0.10–2.0 mg mL^{-1} in 50 mmol L^{-1} pH 8.0 Tris–HCl buffer) and allowed to react for 30 min at 40 °C. Kinetic parameters, including k_{cat}, *K*m, and catalytic efficiency (k_{cat}/*K*m), were fitted non-linearly using GraphPad Prism 5.

To compare the ability of WT BpIH and its mutants to hydrolyze IBI, a bioconversion experiment was conducted. The reaction mixture consisted of 35 g L^{-1} IBI, 50 mmol L^{-1} Tris–HCl, and 75 g L^{-1} wet cells in a volume of 200 mL.

The temperature was maintained at 40 °C, and the pH of the reaction mixture was adjusted to 8.0 using 1 mol L^{-1} NaOH. At defined intervals, the reaction mixture was sampled and diluted with a mobile phase. After centrifugation, the supernatant was analyzed using HPLC.

HPLC analysis

The concentrations of IBI and IBM were analyzed using HPLC. The analysis was performed using a COSMOSIL 5C18-AR-II column (250 mm × 4.6 mm) at a temperature of 30 °C. The mobile phase consisted of a mixture of acetonitrile–water (3.5:6.5, v/v) and 1% (v/v) phosphoric acid, and the flow rate was set to 0.5 mL min^{-1}. The detection wavelength was 210 nm. The retention time for IBM was determined to be 7.2 min, while IBI had a retention time of 15.8 min.

The optical purity of the samples was determined using chiral HPLC with a Chiralpak IG-3 column (3 µm, 4.6 ID × 250 mm). The mobile phase consisted of acetonitrile–water (1:1, v/v), with the pH adjusted to 2.5 using phosphoric acid. The flow rate was 1 mL min^{-1}, and the detection wavelength was 210 nm. Prior to analysis, the samples were derivatized following the method described by Nojiri et al. (Nojiri et al. 2015). A 10-mL derivatization tube was used, containing 510 µL of acetonitrile, 30 mg of potassium carbonate, and 10 mg of benzoylmethyl bromide. The mixture was brought to a final volume of 8.0 mL with the mobile phase. Next, 2 mL of the IBM sample solution (approximately 8 g L^{-1}) was added. The resulting mixture was vortexed for 15 min and allowed to react at room temperature for 4 h. After centrifugation, the supernatant was analyzed using chiral HPLC. The retention times for *S*-IBM and *R*-IBM were found to be 11.5 min and 13.3 min, respectively.

Molecular dynamics studies

MD simulations were performed using GROMACS 4.5.4 with the OPLS-AA/L force file and SPC/E water model (Pronk et al. 2013). WT BpIH and YHS-I mutant molecules were maintained as neutral systems by injecting water molecules and adding opposite charges. The protein was solvated in a cubic box of water, and the edge of the box was approximately 10 Å. Wild-type BpIH and the YHS-I mutant were solvated with 17,170 and 18,136 water molecules, respectively. Eight and nine sodium ions were added to the WT and YHS-I systems, respectively, to maintain neutrality. The LINCS algorithm was used to constrain bonds involving hydrogen atoms. The particle mesh Ewald (PME) method was used to calculate long-range electrostatic interactions. Prior to the MD simulations, each system was energy minimized using the steepest descent method with 50,000 steps. Equilibration was performed for 1 ns, and the temperature was held constant at 313.15 K (40 °C). For the isothermal and isobaric (NPT) systems, a Parrinello–Rahman thermostat and a V-rescale thermostat were used to control pressure and temperature, respectively. For data analysis, a 40-ns MD simulation was performed with a time step of 2 fs, and coordinates were stored every 10 ps for subsequent analysis. The root mean square deviation (RMSD) and root mean square fluctuation (RMSF) values were calculated from the equilibrium state.

Results

Modeling and docking

In the absence of a crystal structure for BpIH, we selected the *Burkholderia pseudomallei* polysaccharide deacetylase family protein (PDB ID: 3S6O) as a template for homology modeling. This protein exhibits a high amino acid sequence identity of 91.03% with BpIH, making it a suitable structural reference. The resulting homology structure model was assessed by SAVES v6.0 (https://saves.mbi.ucla.edu/), and 88.3% of the residues were in most favored regions and 11.3% in additional allowed regions (Fig. S1). The overall quality factor was 96.49%, suggesting the model was reasonable.

The model of BpIH was a tetramer, with an overall shape resembling a rotating saucer (Fig. 1a). When docked with IBI with a grid box nearly covering subunit A, four probable positions were discovered as IBI binding sites (Fig. 1b). At position 1, IBI interacted with residue Asp192 through a hydrogen bond (Fig. 1c), while at position 2, IBI interacted with residues Trp131, His127, Glu38, Asn36, and Asn220 through hydrogen bonds (Fig. 1d). Positions 3 and 4 were located on the surface of the protein, where IBI interacted with Glu108, Arg109, and Glu77 (Fig. 1e and 1f). Position 2 was in a slit pocket of BpIH and shared the same catalytic triad (E38-H127-W131) as the allantoinase PuuE. Furthermore, the amino acid sequence identity between BpIH and PuuE from *Pseudomonas fluorescens* (GenBank: ACA50280.1, PDB: 3CL6) was 61.07% (Fig. S2), suggesting potential similarities in their catalytic mechanisms.

Using substrate docking, 17 amino acids located within a 5 Å radius of the substrate at the active cavity of the protein were identified. These amino acid residues included N36, E38, F55, L56, F101, H127, W131, Y165, G167, R168, Y190, Y215, L217, N220, M222, H263, and R265 (Fig. 2).

Alanine scanning mutagenesis of amino acids within 5 Å of the substrate

To investigate the functional significance of the identified residues, the 17 amino acids within a 5 Å radius of the substrate were mutated to alanine. WT BpIH and mutant

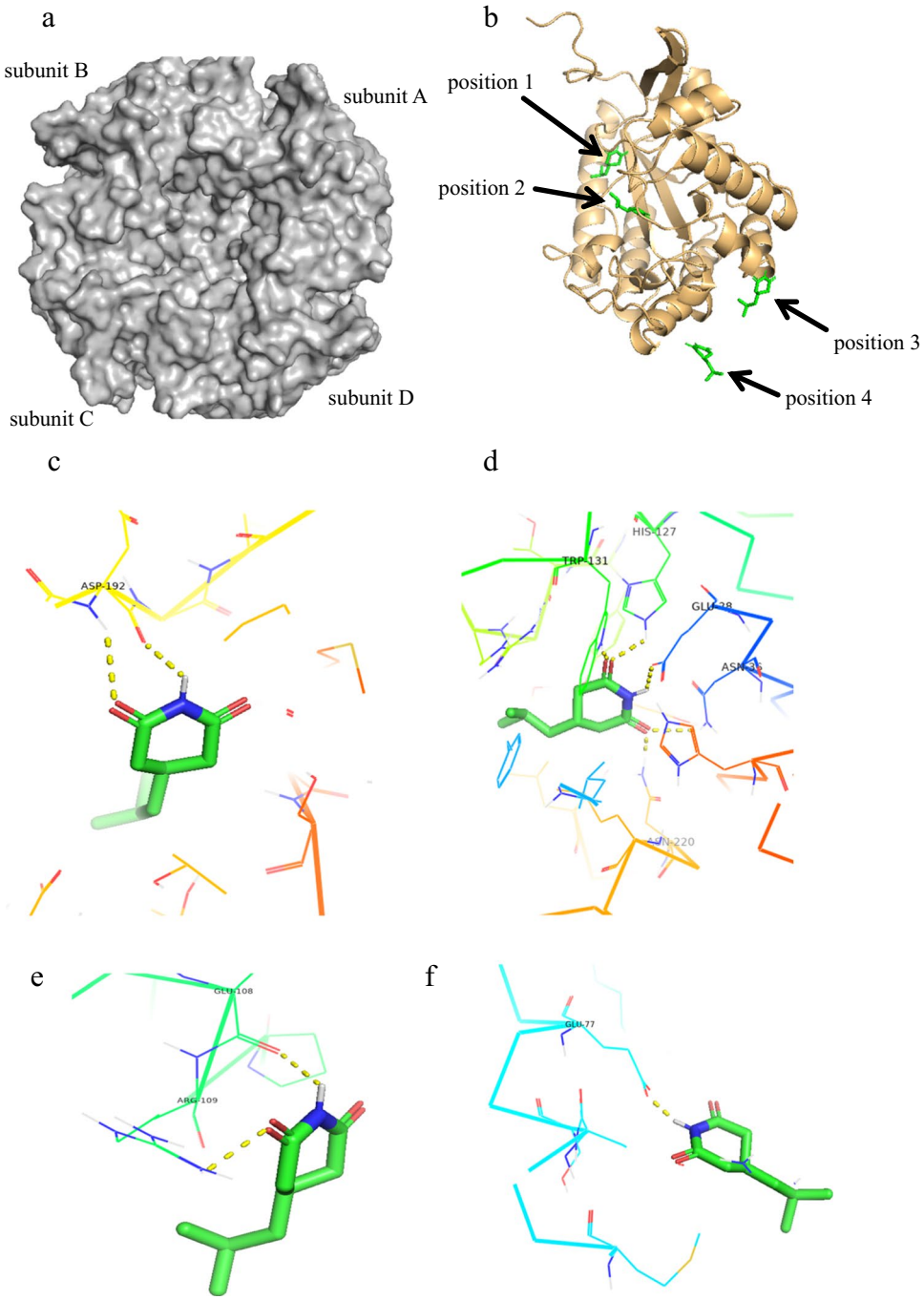

Fig. 1 Binding diagram of IBI with BpIH. **a** Overall structure of the homotetramer BpIH. **b** Four spatial positions of IBI in BpIH subunit A according to the docking results. **c** Interaction of IBI with BpIH in position 1. **d** Interaction of IBI with BpIH in position 2. **e** Interaction of IBI with BpIH in position 3. **f** Interaction of IBI with BpIH in position 4. The substrate IBI is shown as sticks

proteins were expressed in *E. coli*, and crude enzyme solutions were used as catalysts to assess their activity using IBI as a substrate. Protein expression levels between WT BpIH and mutant strains were comparable (Fig. S3), but all alanine mutants exhibited lower enzyme activity compared to the WT (Fig. 3a). Furthermore, substitutions of aromatic residues with alanine, such as H127A and R265A, caused an almost complete loss of catalytic activity, underscoring the crucial role of these amino acids in mediating the reaction.

Interestingly, G167A and W131A mutants retained around 90% and 60% of their activity, respectively. To explore this finding further, semi-saturation mutagenesis was conducted on G167 and W131 (Fig. 3b). The results indicated that most mutants of these two residues exhibited reduced specific enzyme activity, with only G167W, G167I, and G167R mutants showing slightly higher activity than the WT protein. These findings suggest that while mutations at G167 and W131 impact enzyme activity, only specific substitutions may lead to improvements.

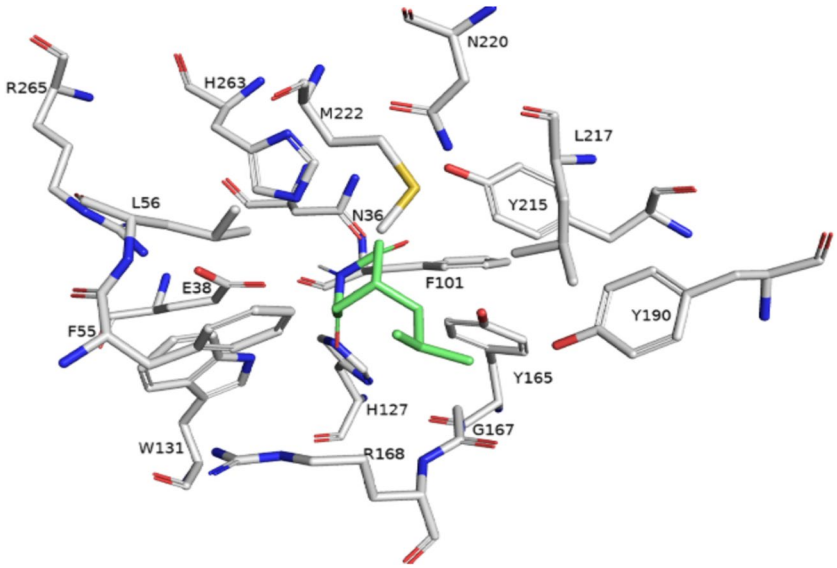

Fig. 2 Model structure of the 17 residues within 5 Å of the substrate IBI. The red circles represent oxygen atoms, the blue circles represent nitrogen atoms, and the green circles represent carbon atoms

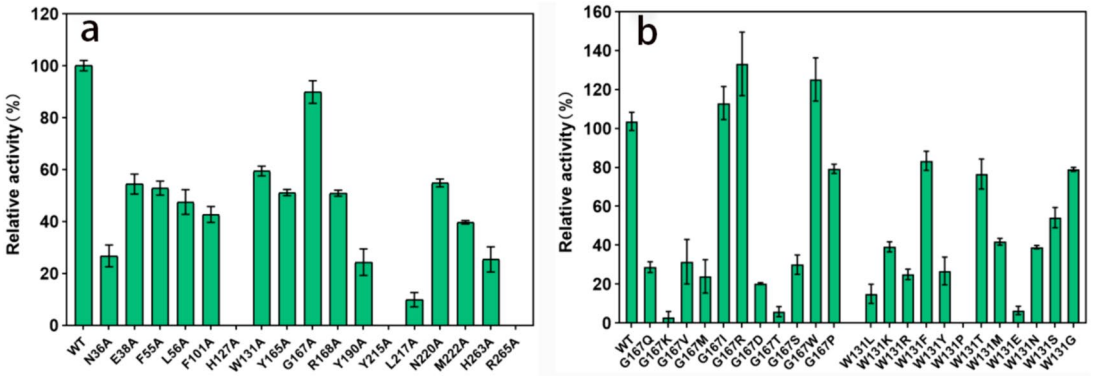

Fig. 3 Enzyme activity determination of WT BpIH and mutants. **a** Alanine scanning of 17 residues within 5 Å of the substrate (IBI). **b** Semi-saturated mutagenesis of G167 and W131

To understand the limited success of the alanine scanning approach on these 17 residues, we conducted a sequence comparison analysis between BpIH and 35 allantoinases that exhibited 50–90% homology with BpIH (Fig. 4a and Table S2). The results revealed a high degree of conservation of these 17 residues in all the allantoinases tested (Fig. 4b). This finding provided a partial explanation for the observed decrease in enzyme activity when G167 and W131 were substituted with amino acids other than alanine. The conservation of these residues among these enzymes suggests their importance in maintaining the structural and functional integrity of the binding pocket. Consequently, substitutions at these positions may disrupt critical interactions necessary for efficient catalysis.

Mutagenesis of residues 6–9 Å from the substrate via semi-rational design

We then redirected our focus to the 16 residues 6–9 Å from the substrate. These residues contacted the substrate indirectly and influenced the catalytic activity of the enzyme through various bonding interactions or structural alterations. As expected, these 16 residues exhibited lower conservation levels compared to the 17 residues within 5 Å of the substrate (Fig. 4b). For example, in the 35 allantoinase PuuEs that were compared, the probability of serine residues at position 226 was even lower than that of leucine and threonine.

Subsequently, a semi-rational mutation library was constructed by replacing the 16 residues with amino acids that

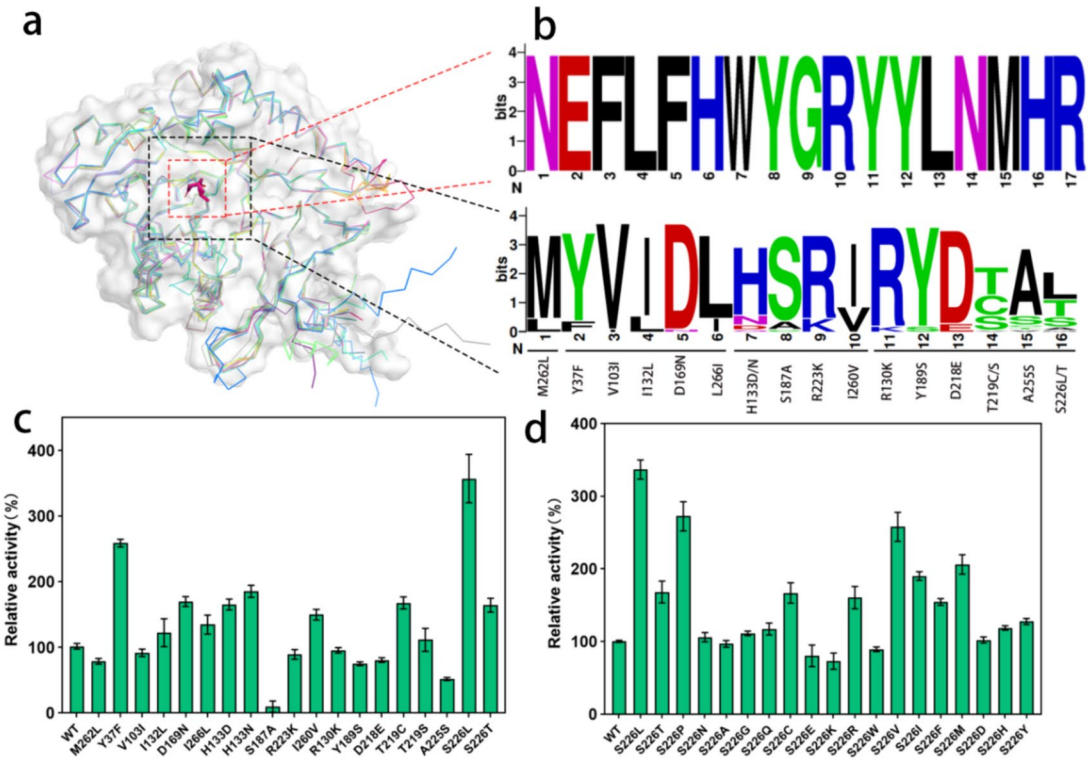

Fig. 4 Conservation analysis of residues within 9 Å and site-directed mutagenesis of residues within 6–9 Å of the binding pocket. **a** Structure superimposition of WT BpIH and the allantoinase family proteins. **b** Conservativity analysis of the residues within 5 Å (upper) and 6–9 Å (lower) of the binding pocket. The letter size represents the degree of conservation of the residue. **c** Relative activity of WT BpIH and mutants of residues within 6–9 Å of the binding pocket. **d** Relative activity of WT BpIH and mutants of S226

also occurred frequently based on the sequence comparisons. Interestingly, numerous mutants exhibited higher specific enzyme activity than the WT. Notably, mutants Y37F, H133N, and S226L demonstrated specific enzyme activity of 2.1, 1.5, and 3.0 U g^{-1}, respectively. These values corresponded to 1.5-fold, 0.8-fold, and 2.5-fold increases over WT BpIH, respectively (Fig. 4c). Furthermore, the specific enzyme activity of the S226T mutant was 0.7-fold higher than that of WT BpIH, indicating that S226 is a key residue, prompting us to perform saturated mutagenesis at this position.

As anticipated, many of the mutants exhibited significantly enhanced specific enzyme activities compared to that of WT BpIH (Fig. 4d). In addition to S226L, the specific activities of S226P, S226I, and S226V were found to be 1.7-fold, 0.9-fold, and 1.5-fold higher than that of the WT, respectively. These findings further underscored the importance of residue S226 in modulating enzyme activity and provided potential candidates for subsequent optimization of the enzyme's performance through targeted mutagenesis.

To explore potential epistatic interactions among these mutants (Qu et al. 2021), we introduced additional combinatorial mutations that exhibited enhanced activity. Most of the combined mutants did not exhibit any further increase in specific activity, and some even showed a slight decrease (data not shown). However, a few mutants demonstrated an improvement in specific activity (Fig. 5). Notably, the YHS-I triple mutant exhibited the highest specific activity, reaching 5.1 U g^{-1}, which was 5.0-fold higher than that of WT BpIH.

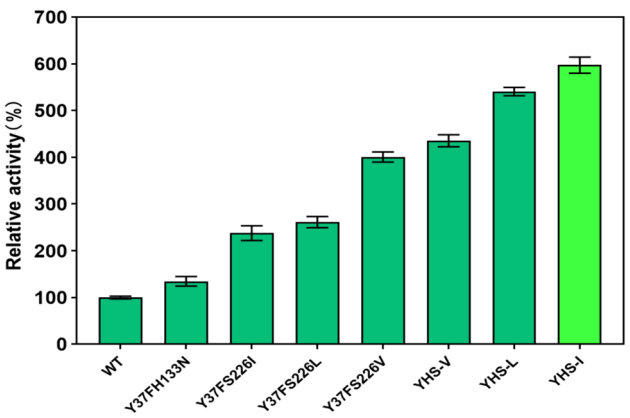

Fig. 5 Comparison of the activity of WT BpIH and the combinatorial mutants of residues Y37, H133, and S226. The relative specific enzyme activity of YHS-I is shown in lime green, and the remaining mutant strains are shown in green. YHS-V, Y37FH133NS226V; YHS-I, Y37FH133NS226I; YHS-L, Y37FH133NS226L

Kinetic analysis and bioconversion of IBI

To assess the impact of the mutations on the enzyme's kinetic properties, a comparison was made between WT BpIH and several of its mutants (Table 1). Remarkably, the YHS-I mutant exhibited the lowest *K*m value and the highest k_{cat} value, indicating a substantially improved affinity and catalytic efficiency toward IBI. In addition, both the YHS-L and S226L mutants exhibited higher catalytic efficiencies (k_{cat}/*K*m) than WT BpIH, despite having similar *K*m values (Table 1). These findings provided compelling evidence that the directed evolutionary approach used to modify BpIH led to significant enhancements in its catalytic efficiency for IBI. The improvements observed in both affinity and catalytic efficiency indicated the successful optimization of the enzyme's performance by applying targeted mutagenesis. These results underscore the potential of rational design strategies to engineer enzymes with enhanced biochemical properties.

The production efficiencies of *R*-IBM of the mutants YHS-I, YHS-L, and S226L and of WT BpIH were compared. All the mutants exhibited a superior ability to produce IBM compared to WT BpIH. Among them, the YHS-I mutant demonstrated outstanding results, achieving an IBM conversion rate of 88.87% within 48 h of the reaction, while WT BpIH had a conversion rate of only 38.15% (Fig. 6). Importantly, all the IBM products synthesized by these mutants were exclusively of the *R* isomer form, with *ee* values exceeding 99.9% (Table 1, Fig. S4). These results confirm that the chiral selectivity of these mutants did not decrease.

Molecular dynamics of WT BpIH and the highest performing mutant, YHS-I

For insights into how the altered residues in the mutants impacted the catalytic efficiency of BpIH, molecular dynamics (MD) simulations were conducted at 313.15 K (40 °C) over a 40-ns time scale to observe the dynamic behavior of the enzymes. The RMSD values stabilized after approximately 15 ns. The average RMSD values for

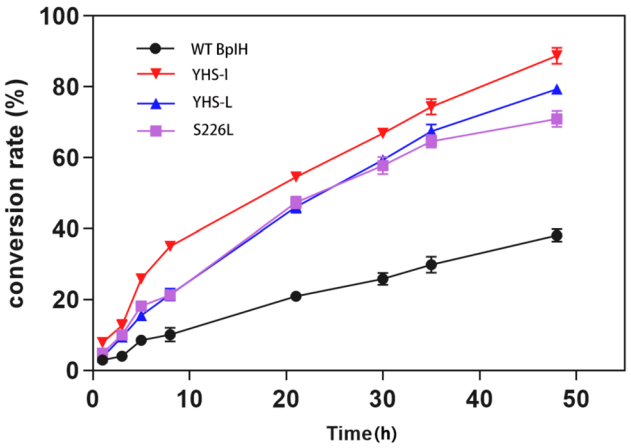

Fig. 6 *R*-IBM conversion from IBI catalyzed by WT BpIH and three mutants (S226L, YHS-L, and YHS-I)

WT BpIH and the YHS-I mutant in the equilibrium structure were similar, with values of 0.291 nm and 0.289 nm, respectively (Fig. 7a). This suggests that both WT BpIH and the YHS-I mutant likely had similar conformations and stabilities. Stability tests performed at 40 °C demonstrated that both enzymes had similar stability curves (Fig. 7c).

In addition, RMSF analysis was used to investigate the flexibility differences among residues in the WT BpIH and YHS-I mutant proteins. The overall RMSF values were similar, with differences in the mutated residue regions. Notably, in the proximity of H133N and S226I residues, the RMSF values decreased from 0.11 nm and 0.20 nm to 0.06 nm and 0.10 nm, respectively (Fig. 7b). These results indicated a reduction in fluctuations and an increase in local stability at these specific locations.

The average structures were extracted from the last 10 ns of the equilibrated state in the MD simulations (Fig. 7d). The overall structure of the YHS-I mutant remained largely unchanged; however, significant local changes were observed in the active site architecture, which likely contributed to the enhanced catalytic efficiency of the mutant.

Table 1 Kinetic parameters and enantiopurity of WT BpIH and its mutants

	k_{cat} (min^{-1})	*K*m (mmol L^{-1})	k_{cat}/*K*m (min^{-1})	ee_p (%)[a]
WT BpIH	0.58 ± 0.45	9.02 ± 0.51	0.064 ± 0.05	99.96 ± 0.02 (*R*)
S226L	3.10 ± 0.37	9.28 ± 1.09	0.328 ± 0.07	99.96 ± 0.02 (*R*)
Y37FH133NS226L	3.12 ± 0.22	8.48 ± 1.03	0.340 ± 0.07	99.91 ± 0.03 (*R*)
Y37FH133NS226I	3.44 ± 0.30	7.31 ± 0.73	0.469 ± 0.06	99.90 ± 0.04 (*R*)

Abbreviation: ee_p, enantiomeric excess of product.

[a]The enantioselectivity of the product (*R*)-3-isobutylglutarate monoamide (*R*-IBM) was determined by benzoylmethyl bromide derivatization, which was repeated three times using the catalytic product of each mutant. $ee_R\% = (R-S)/(R+S) \times 100\%$

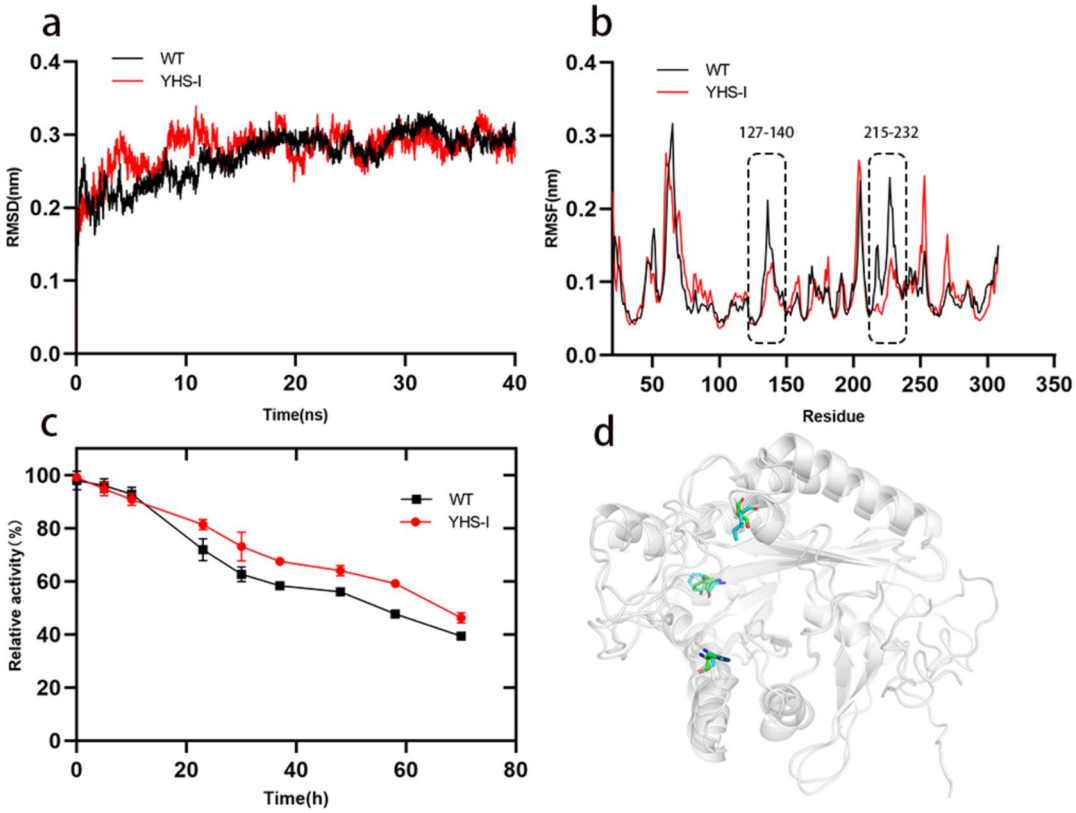

Fig. 7 Molecular dynamics study of WT BpIH and the YHS-I mutant. MD simulations were performed over a 40-ns time period at 40 °C. **a** RMSD. **b** RMSF. **c** Stability at 40 °C. Each experiment was repeated three times. **d** Overlay of the average structures extracted from the final 10 ns of the equilibrated state of the MD simulations, with proteins shown in cartoon form (white) and mutant site residues shown in stick form (green)

Discussion

Directed evolution has emerged as a valuable tool for enhancing the performance of catalysts in pregabalin biosynthesis, such as lipase (Ding et al. 2018), nitrilase (Zhang et al. 2020), and D-hydantoinase. The engineered D-hydantoinase was shown to be capable of synthesizing *R*-IBM with a 99% molar yield and 99.8% *ee* in a kilogram-scale synthesis (Liu et al. 2022). In addition to hydantoinase, the imidase BpIH is also a promising enzyme for producing *R*-IBM industrially, but its enzyme activity must be significantly increased.

Through homology modeling and molecular docking, the catalytic triad of BpIH was speculated to be E38-H127-W131, and 17 amino acids were found to be located within a 5 Å radius of the substrate at the active cavity of the protein. Attempts were made to improve the enzyme–substrate interactions by mutating these 17 residues, but alanine scanning and semi-saturated mutagenesis did not yield mutants with significant improvements. Further comparisons of BpIH and 35 allantoinases with 50–90% homology with the BpIH sequence revealed that these 17 residues were highly conserved. Allantoinase is a key enzyme in purine metabolism, and this high level of conservation perhaps was important in evolution.

Instead, we found that the catalytic activity of this enzyme was significantly improved by mutating the 16 residues that contacted the substrate indirectly. These residues were located 6–9 Å from the substrate molecule, were less conserved, and interacted with the substrate indirectly. It is interesting that the chiral selectivity of all mutations of this study, including the highest performing mutant YHS-I, was very high with *ee* > 99%. One possible reason is that instead of performing saturation mutagenesis on these amino acids, we only replaced them with residues frequently appearing in other PuuE allantoinases. PuuE shows strict stereoselectivity (Ramazzina et al. 2008), and PuuE from *P. fluorescens* (GenBank: ACA50280.1) exhibited 63% identity with allantoinase AfIH, which also catalyzed the hydrolysis of IBI with high *R*-stereoselectivity (Cai et al. 2023; Liu et al. 2022; Nojiri et al. 2015, 2013). This semi-rational strategy also helped to improve the efficiency of finding desirable mutations; otherwise, significant tedious work would have been needed

to isolate mutants with high *ee* values for *R*-IBM production, as changes occurring outside the active site can also play a crucial role in enzyme enantioselectivity. For example, the Y14W mutant exhibited a stereoselectivity of 93.70%, whereas the I260V mutant exhibited a significantly reduced stereoselectivity of only 20.78% (Fig. S5).

The MD simulation partially explained the increased catalytic activity of the YHS-I mutant. The simulation result showed a reduction in fluctuations and an increase in the stability in the mutated regions of H133N and S226I. The substitution of hydrophilic residues with non-hydrophilic N and I may have increased the rigidity of these two sites, influencing substrate binding and contributing to the improved catalytic efficiency. The link between increased activity and enhanced rigidity at mutation sites has also been reported recently (Lv et al. 2021; Torktaz et al. 2018).

Despite a fivefold increase in the activity of BpIH in this study, there is still additional room for further modifications of the enzyme, such as saturation mutations of the residues 6–9 Å from the substrate, mutations of residues even further from the substrate, and other mutations. Moreover, the template we selected for homologous modeling (PDB ID: 3S6O) is tetramer trimer; however, BpIH is a trimer. This may lead to significant errors in the predicted structure, posing significant challenges for the rational design of enzymes. This study only enhanced the activity of BpIH, and further research is needed to improve its stability and other parameters affecting catalytic performance.

Supplementary Information The online version contains supplementary material available at https://doi.org/10.1007/s00253-024-13311-2.

Acknowledgements We thank Dr. Haiyang Xia and Dr. Yusi Yan for their excellent support in protein structure analysis and site-directed mutagenesis. We acknowledge Engineer Minjie Wang for her strong support on the assistance of optical selectivity determination. We thank engineer Shanshan Tian for her assistance during strain fermentation. We thank LetPub (www.letpub.com.cn) for its linguistic assistance during the preparation of this manuscript.

Author contribution WQ is the first author responsible for article conceptualization, formal analysis, and writing—original draft. LX is responsible for formal analysis. KC is responsible for formal analysis and software. YL is responsible for supervision and writing—review and editing. ZY is responsible for funding acquisition, methodology, resources, validation, and writing—review and editing.

Data availability The sequences of the imidase BpIH and allantoinase PuuE family proteins mentioned in this study are available from the National Centre for Biotechnology Information (NCBI).

Declarations

Ethical approval This article does not contain any studies with human participants or animals performed by any of the authors.

Consent for publication All the authors read and agree the content of this paper and its publication.

Competing interests The authors declare no competing interests.

References

Arnold K, Bordoli L, Kopp J, Schwede T (2006) The SWISS-MODEL workspace: a web-based environment for protein structure homology modelling. Bioinformatics 22(2):195–201. https://doi.org/10.1093/bioinformatics/bti770

Bockbrader HN, Wesche D, Miller R, Chapel S, Janiczek N, Burger P (2010) A comparison of the pharmacokinetics and pharmacodynamics of pregabalin and gabapentin. Clin Pharmacokinet 49(10):661–669. https://doi.org/10.2165/11536200-000000000-00000

Bradford M (1976) A rapid and sensitive method for the quantitation of microgram quantities of protein utilizing the principle of protein-dye binding. Anal Biochem 72(1–2):248–254. https://doi.org/10.1016/0003-2697(76)90527-3

Cai QF, Qin WP, Yang ZY, Xu L, Wang YL, Fang JY, Lu YH (2023) Preparation of pregabalin intermediate (*R*) -isobutylglutarate monoamide with imidase. Journal of Shenyang Pharmaceutical University 40(5):0649–06. https://doi.org/10.14066/j.cnki.cn21-1349/r. 2021.0840

Chen M, Song F, Qin Y, Han S, Rao Y, Liang S, Lin Y (2022) Improving thermostability and catalytic activity of glycosyltransferase from *Panax ginseng* by semi-rational design for rebaudioside D synthesis. Frontiers Bioeng Biotechnol 10:884898. https://doi.org/10.3389/fbioe.2022.884898

Crooks GE, Hon G, Chandonia J-M, Brenner SE (2004) WebLogo: a sequence logo generator: Figure 1. Genome Res 14(6):1188–1190. https://doi.org/10.1101/gr.849004

Ding X, Zheng RC, Tang XL, Zheng YG (2018) Engineering of *Talaromyces thermophilus* lipase by altering its crevice-like binding site for highly efficient biocatalytic synthesis of chiral intermediate of Pregablin. Bioorg Chem 77:330–338. https://doi.org/10.1016/j.bioorg.2018.01.018

Gray P (2007) Pregabalin in the management of central neuropathic pain. Expert Opin Pharmacother 8(16):3035–3041. https://doi.org/10.1517/14656566.8.17.3035

Holmquist M (2000) Alpha/beta-hydrolase fold enzymes: structures, functions and mechanisms. Curr Protein Pept Sci 1:209–235. https://doi.org/10.2174/1389203003381405

Huang C-Y (2020) Structure, catalytic mechanism, posttranslational lysine carbamylation, and inhibition of dihydropyrimidinases. Adv

Protein Chem Struct Biol 122:63–96. https://doi.org/10.1016/bs.apcsb.2020.05.002

Jitonnom J, Lomthaisong K, Lee VS (2012) Computational design of peptide inhibitor based on modifications of proregion from *Plutella xylostella* midgut trypsin. Chem Biol Drug Des 79(4):583–593. https://doi.org/10.1111/j.1747-0285.2011.01312.x

Larkin MA, Blackshields G, Brown NP, Chenna R, McGettigan PA, McWilliam H, Valentin F, Wallace IM, Wilm A, Lopez R, Thompson JD, Gibson TJ, Higgins DG (2007) Clustal W and Clustal X version 2.0. Bioinformatics 23(21):2947–2948. https://doi.org/10.1093/bioinformatics/btm404

Liu F, Ren J, Guo L, Liu Y, Li D-F, Yu B (2022) Desymmetric hydrolysis of prochiral imide for S-pregabalin synthesis by rationally designed D-hydantoinase. Green Chem 24(12):4748–4753. https://doi.org/10.1039/d2gc00728b

Lv K, Shao W, Pedroso MM, Peng J, Wu B, Li J, He B, Schenk G (2021) Enhancing the catalytic activity of a GH5 processive endoglucanase from *Bacillus subtilis* BS-5 by site-directed mutagenesis. Int J Biol Macromol 168:442–452. https://doi.org/10.1016/j.ijbiomac.2020.12.060

Martínez-Rodríguez S, Martínez-Gómez AI, Clemente-Jiménez JM, Rodríguez-Vico F, García-Ruíz JM, Las Heras-Vázquez FJ, Gavira JA (2010) Structure of dihydropyrimidinase from *Sinorhizobium meliloti* CECT4114: new features in an amidohydrolase family member. J Struct Biol 169(2):200–208. https://doi.org/10.1016/j.jsb.2009.10.013

Meelua W, Wanjai T, Thinkumrob N, Oláh J, Cairns JRK, Hannongbua S, Ryde U, Jitonnom J (2023) A computational study of the reaction mechanism and stereospecificity of dihydropyrimidinase. Phys Chem Chem Phys 25(12):8767–8778. https://doi.org/10.1039/d2cp05262h

Min K, Kim H, Park HJ, Lee S, Jung YJ, Yoon JH, Lee JS, Park K, Yoo YJ, Joo JC (2021) Improving the catalytic performance of xylanase from *Bacillus circulans* through structure-based rational design. Bioresour Technol 340:125737. https://doi.org/10.1016/j.biortech.2021.125737

Morris GM, Huey R, Lindstrom W, Sanner MF, Belew RK, Goodsell DS, Olson AJ (2009) AutoDock4 and AutoDockTools4: automated docking with selective receptor flexibility. J Comput Chem 30(16):2785–2791. https://doi.org/10.1002/jcc.21256

Nojiri M, Uekita K, Ohnuki M, Taoka N, Yasohara Y (2013) Microbial asymmetric hydrolysis of 3-substituted glutaric acid diamides. J Appl Microbiol 115(5):1127–1133. https://doi.org/10.1111/jam.12309

Nojiri M, Hibi M, Shizawa H, Horinouchi N, Yasohara Y, Takahashi S, Ogawa J (2015) Imidase catalyzing desymmetric imide hydrolysis forming optically active 3-substituted glutaric acid monoamides for the synthesis of gamma-aminobutyric acid (GABA) analogs. Appl Microbiol Biotechnol 99(23):9961–9969. https://doi.org/10.1007/s00253-015-6812-x

Ogawa J, Chee-Leong S, Horinouchi N, Nojiri M, Takeuchi M, Hibi M (2019) Microbial cyclic imide metabolism and its biotechnological application. Imides:65–90. https://doi.org/10.1016/B978-0-12-815675-9.00003-5

Pronk S, Páll S, Schulz R, Larsson P, Bjelkmar P, Apostolov R, Shirts MR, Smith JC, Kasson PM, van der Spoel D, Hess B, Lindahl E (2013) GROMACS 4.5: a high-throughput and highly parallel open source molecular simulation toolkit. Bioinformatics 29(7):845–854. https://doi.org/10.1093/bioinformatics/btt055

Qu G, Bi Y, Liu B, Li J, Han X, Liu W, Jiang Y, Qin Z, Sun Z (2021) Unlocking the stereoselectivity and substrate acceptance of enzymes: proline-induced loop engineering test. Angewandte Chemie Int Ed 61(1). https://doi.org/10.1002/anie.202110793

Ramazzina I, Cendron L, Folli C, Berni R, Monteverdi D, Zanotti G, Percudani R (2008) Logical identification of an allantoinase analog (puuE) recruited from polysaccharide deacetylases. J Biol Chem 283(34):23295–23304. https://doi.org/10.1074/jbc.M801195200

Silverman RB (2008) From basic science to blockbuster drug: the discovery of Lyrica. Angew Chem Int Ed Engl 47(19):3500–3504. https://doi.org/10.1002/anie.200704280

Tassone DM, Boyce E, Guyer J, Nuzum D (2007) Pregabalin: a novel 7-aminobutyric acid analogue in the treatment of neuropathic pain, partial-onset seizures, and anxiety disorders. Clin Ther 29(1):26–48. https://doi.org/10.1016/j.clinthera.2007.1.013

Torktaz I, Karkhane AA, Hemmat J (2018) Rational engineering of Cel5E from *Clostridium thermocellum* to improve its thermal stability and catalytic activity. Appl Microbiol Biotechnol 102(19):8389–8402. https://doi.org/10.1007/s00253-018-9204-1

Tue-Ngeun P, Rakitikul W, Thinkumrob N, Hannongbua S, Meelua W, Jitonnom J (2024) Binding interactions and in silico ADME prediction of isoconessimine derivatives as potent acetylcholinesterase inhibitors. J Mol Graph Model 129:108746. https://doi.org/10.1016/j.jmgm.2024.108746

Wu X, Tian Z, Jiang X, Zhang Q, Wang L (2018) Enhancement in catalytic activity of Aspergillus niger XynB by selective site-directed mutagenesis of active site amino acids. Appl Microbiol Biotechnol 102(1):249–260. https://doi.org/10.1007/s00253-017-8607-8

Wu L, Qin L, Nie Y, Xu Y, Zhao YL (2022) Computer-aided understanding and engineering of enzymatic selectivity. Biotechnol Adv 54:107793. https://doi.org/10.1016/j.biotechadv.2021.107793

Xu Z, Cen YK, Zou SP, Xue YP, Zheng YG (2020) Recent advances in the improvement of enzyme thermostability by structure modification. Crit Rev Biotechnol 40(1):83–98. https://doi.org/10.1080/07388551.2019.1682963

Zhang Q, Lu XF, Zhang Y, Tang XL, Zheng RC, Zheng YG (2020) Development of a robust nitrilase by fragment swapping and semi-rational design for efficient biosynthesis of pregabalin precursor. Biotechnol Bioeng 117(2):318–329. https://doi.org/10.1002/bit.27203

Zheng W, Pu Z, Xiao L, Xu G, Yang L, Yu H, Wu J (2023) Mutability-landscape-guided engineering of l-threonine aldolase revealing the prelog rule in mediating diastereoselectivity of C-C bond formation. Angew Chem Int Ed Engl 62(2):e202213855. https://doi.org/10.1002/anie.202213855